arXiv:1410.3146v1 [astro-ph.GA] 12 Oct 2014

UV spectral diagnostics for low redshift quasars: estimating physical conditions and radius of the Broad Line Region

**P. Marziani • J. W. Sulentic • C. A. Negrete •
D. Dultzin • A. Del Olmo •
M. A. Martínez Carballo • T. Zwitter • R. Bachev**

Abstract The UV spectral range (1100 – 3000 Å) contains the strongest resonance lines observed in active galactic nuclei (AGN). Analysis of UV line intensity ratios and profile shapes in quasar spectra provide diagnostics of physical and dynamical conditions in the broad line emitting region. This paper discusses properties of UV lines in type-1 AGN spectra, and how they lead an estimate of ionizing photon flux, chemical abundances, radius of the broad line emitting region and central black hole mass. These estimates are meaningfully contextualised through the 4D "eigenvector-1" (4DE1) formalism.

Keywords galaxies: active; quasars: emission lines; quasars: general; techniques: spectroscopic; astronomical databases: surveys

P. Marziani
INAF, Osservatorio Astronomico di Padova, Padova, Italia
J. W. Sulentic
Instituto de Astrofísica de Andalucía (CSIC), Granada, Spain
C. A. Negrete
INAOE, Tonantzintla, Puebla, Mexico
D. Dultzin
Instituto de Astronomía, UNAM, Mexico, D.F., Mexico
A. Del Olmo
Instituto de Astrofísica de Andalucía (CSIC), Granada, Spain
M. A. Martínez Carballo
Instituto de Astrofísica de Andalucía (CSIC), Granada, Spain
T. Zwitter
University of Ljubljana, Faculty of Mathematics and Physics, Ljubljana, Slovenia
R. Bachev
Bulgarian Academy of Science, Sofia, Bulgaria

1 Introduction

It is now roughly 35 years since the International Ultraviolet Explorer (IUE) opened the possibility to study UV spectra of Seyfert nuclei and broad line radio galaxies thus revealing strong similarities between low- and high-redshift quasars (where the UV lines are redshifted into the optical domain). IUE data helped to establish that active galactic nuclei (AGN) involved sources spanning an enormous range of luminosity but driven by the same underlying process involving accretion onto a massive compact object, most likely a black hole (see e.g., Chapter 1 of D'Onofrio et al. 2012). The advent of HST in 1991 made possible observations of even fainter AGN and with unprecedented resolution (comparable to the best ground based optical spectra). HST archival observations continue to provide a database from which much AGN research is being carried out. Important information about density, ionization conditions, and dynamics in the (especially high-ionization) broad line emitting region (HIL–BLR) of AGN can be inferred from UV spectroscopic observations (§2 and §3). It is useful to point out three factors affecting our ability to achieve these goals.

- The line emitting regions in type-1 AGN are spatially unresolved in even the nearest AGN. This is an important reason why modeling the structure of the inner regions of quasars remains an open issue (see Netzer 2013 and Gaskell 2009). Much effort has gone into measuring the size of the broad line emitting regions (BLR) from time lags in the response of emission lines to continuum change (Peterson et al. 2004). Work has also focussed on constraining the BLR structure using velocity-resolved emission line profiles (Grier et al. 2013, and references therein).
- AGN spectral properties show considerable diversity. The point is that type-1 AGN spectra are not self-similar nor do they scatter with low dispersion

around an average spectrum (Sulentic et al. 2002; Bachev et al. 2004). If they did then we would not need the contextualization described in §3, just as we would not need an H-R diagram if all stars were of the same spectral type. Type-1 AGN actually show large multi-wavelength diversity ranging from Narrow Line Seyfert 1 (NLSy1) to Broad Line Radio Galaxies (BLRG). These two extremes involve sources whose emitting regions are empirically and physically very different. Attempts to explain them with a single model will yield misleading results (Sulentic et al. 2000, 2002).

- Finally we point out that the availability of UV spectra is limited and that this is an impediment to further progress in quasar studies involving comparisons of low- and high-z AGN (§5). This concerns single epochs observations suitable for statistical studies as well as monitoring for reverberation mapping.

2 The UV Diagnostics

2.1 Prominent UV emission lines

An important property of AGN spectra involves the existence of both high and low ionization lines (hereafter HILs and LILs). By low and high ionization we mean, respectively, lines emitted by ionic species with ionization potential $\lesssim$20 eV (hydrogen, singly ionized ionic species of magnesium, carbon, iron, calcium) and $\gtrsim$ 40 eV (triply ionized carbon, helium, four times ionized nitrogen). An exhaustive list of lines is provided by Vanden Berk et al. (2001). If we confine our studies to the range 1100 – 2000 Å, we observe: (1) the strongest HILs associated with resonance transitions, (2) usually weak LIL emission due to OIλ1304, SiIIλ1814 features and (3) several inter-combination lines from transitions leading to the ground state, most notably, CIII]λ1909, SiIII]λ1892, and the narrow lines of NIII]λ1750 and OIII]λ1663. Once and twice ionized iron emission is not strong between 1200 and 2000 Å although FeIII emission can be significant in the 1900 Å blend whose main components are AlIIIλ1860, SiIII]λ1892, and CIII]λ1909 (Vestergaard and Wilkes 2001). The most notable features that are unblended with stronger lines include the UV multiplet 191 FeII at 1780 Å and an FeIII blend at 2100 Å. It is customary to assume that FeII and, to some extent, FeIII emission maintain the same intensity ratios in all sources. Under this assumption intensity measures of FeII and FeIII at 1780 and 2100 Å define the entire UV emission spectrum due to these ions. This approach (i.e., using a "template" to represent blended emission features spread over a wide wavelength range) is justified within the limit of resolution and S/N presently obtainable for most optical and UV data although the real situation is known to be more complex.

2.2 Line Ratios

Line intensity ratios are sensitive to: (1) density, if one of the lines has a well-defined critical density, (2) ionisation level, with lines coming from transitions occurring in different ionic species of the same element providing the most robust diagnostics, and (3) chemical composition, if ratios involve a metal line and HeIIλ1640 or CIVλ1549. Intensity ratios of broad inter-combination and permitted lines, most notably CIIIλ1909/SiIII]λ1892 and AlIIIλ1860/ SiIII]λ1892 are useful diagnostics for a range of density that depends on their transition probabilities. The CIIIλ1909/ SiIII]λ1892 and AlIIIλ1860/SiIII]λ1892 ratios are suitable as diagnostics for $n_{\rm e} < 10^{11}$ cm^{-3} and $10^{11} - 10^{13}$ cm^{-3} ranges, respectively. The latter range corresponds to the densest, low ionization emitting regions likely associated with production of FeII (Sigut and Pradhan 2003; Brühweiler and Verner 2008). The ratios SiII]λ1814/SiIII]λ1892 and SiIVλ1397/ SiIII]λ1892 are sensitive to the ionization level and have the considerable advantage of being independent of chemical abundance. Ratios CIV λ1549/ AlIII λ1860 and CIV λ1549/ SiIII λ1892 provide information about ionization that is however metallicity dependent. The ratios involving NVλ1240 (NVλ1240/HeIIλ1640 or NVλ1240/CIVλ1549) are strongly sensitive to metallicity if nitrogen is considered a secondary element (Ferland et al. 1996). The ratio (SiIVλ1397+ OIV]λ1402) / CIVλ1549 has also been used as a metallicity indicator (Nagao et al. 2006).

2.3 Photoionization calculations

The emission line ratios reported above provide information about the product of ionization parameter U and hydrogen number density $n_{\rm H}$ if interpreted through a multidimensional grid of photoionization simulations. Quantitative constraints obtained from diagnostic ratios require a-priori knowledge of the principal ionization mechanism and some basic assumptions about the structure of the emitting region. Photoionization is considered the dominant mechanism for HIL and intermediate ionization lines (Davidson and Netzer 1979). Physical conditions of the photoionized gas can be described by: 1) density $n_{\rm H}$ or electron density, 2) hydrogen column density $N_{\rm H}$ 3) metallicity Z, 4) shape of the ionizing continuum and 5) ionization parameter U. U represents the dimensionless ratio of the number of

ionizing photons and the total hydrogen density. Both U and $n_{\rm H}$ are related through the equation

$$U = \frac{\int_{\nu_0}^{+\infty} \frac{L_\nu}{h\nu} d\nu}{4\pi n_{\rm H} c r^2} \quad (1)$$

where L_ν is the specific luminosity per unit frequency, h is the Planck constant, ν_0 the Rydberg frequency, c the speed of light, and r can be interpreted as the distance between the central source of ionizing radiation and the line emitting region. Simulations with CLOUDY (Ferland et al. 2013) were carried out over the density range $7.00 \leq \log n_{\rm H} \leq 14.00$, and $-4.50 \leq \log U \leq 00.00$ (in intervals of 0.25). Each simulation was computed for a fixed ionization parameter and density, assuming plane parallel geometry (i.e., a slab of gas illuminated by the ionizing continuum). The $n - U$ array was computed several times for solar and supersolar chemical compositions, two different continua and column density values $N_{\rm H} = 10^{23}$ (assumed as a standard value), plus $N_{\rm H} = 10^{22}$, 10^{24} cm^{-2}.

Fig. 1 shows the behaviour of SiIII]λ1892/ CIVλ1549 (left panel) and SiIII]λ1892/ AlIIIλ1860 (right panel) in the U vs. $n_{\rm H}$ plane assuming solar metallicity, $N_{\rm H} = 10^{23}$ cm^{-2}, and the standard CLOUDY AGN continuum. As expected the SiIII]λ1892/CIVλ1549 ratio depends on U in a way that is almost independent of density up to the SiIII]λ1892 critical density. The AlIIIλ1860/SiIII]λ1892 ratio increases smoothly with density with an increase that is not strongly dependent on U for $-3.5 \lesssim U \lesssim -1$.

3 Systematic changes along the 4DE1 sequence

Until recently we lacked a contextualization within which the dispersion in optical and UV spectroscopic properties could be organized (e.g. a quasar equivalent of the stellar H-R diagram). There has been recent progress especially if we restrict our attention to type-1 AGN. Spectroscopic measures from large AGN samples can be viewed as defining a parameter space whose axes are not fully orthogonal. A principal component analysis (PCA) can be used to identify the first orthogonal axes (which are expressed as linear combinations of the observed parameters) that account for most of the parameter diversity in a sample. The "first eigenvector" revealed by PCA organizes AGN along a sequence originating in an optical parameter plane FWHM Hβ vs. intensity ratio $R_{\rm FeII}$= FeIIλ4570/Hβ (Boroson and Green 1992). This is the "optical" plane of the 4D eigenvector 1 parameter space (Sulentic et al. 2000) that adds systematic trends involving CIVλ1549 and the soft X-ray photon index (Sulentic et al. 2007). If trends in physical conditions are taken into account it is possible to obtain accurate estimates of the emitting region radius from this data (§4).

Systematic differences along the the eigenvector 1 sequence do not involve only FeII and FWHM Hβ (Zamfir et al. 2010; Popović and Kovačević 2011; Steinhardt and Silverman 2013), but also the spectral energy distribution (Kuraszkiewicz et al. 2009; Tang et al. 2012), X-ray continuum / CIVλ1549 properties (Kruczek et al. 2011), the ratio between optical and UV FeII emission (Sameshima et al. 2011), and, most notably, the ratios AlIIIλ1860/ SiIII]λ1892, and SiIII]λ1892/ CIII]λ1909 (Baldwin et al. 1996; Wills et al. 1999; Bachev et al. 2004). Eddington ratio is considered the main physical driver of the eigenvector 1, with orientation affecting mainly line widths (Marziani et al. 2001; Boroson 2002). Ferland et al. (2009) establish a link between $R_{\rm FeII}$, column density and Eddington ratio along the eigenvector 1 sequence.

Several authors distinguish between two main type-1 AGN populations that involve sources at the opposite ends of the eigenvector 1 sequence, and speak of NLSy1s and broad(er) line quasars (BLQs) or Population A and B(roader) (Sulentic et al. 2000) or Population 1 and 2 (Collin et al. 2006) or disk- and wind-dominated sources (Richards et al. 2011). We adopt the Pop. A and B subdivision involving a boundary at FWHM(Hβ) $\approx$ 4000 km s^{-1} (Sulentic et al. 2007, and references therein).

3.1 Dynamics of the Broad Line Regions

In order to properly interpret intensity ratios it is necessary to understand that HILs and LILs arise from emitting gas not necessarily in the same physical and dynamical conditions (e.g., Sulentic et al. 2007; Richards et al. 2011). HST has made it possible to measure line shifts with an accuracy of $\pm$200 km s^{-1} relative to a quasar rest frame derived from optical observations. The prototypical HIL CIVλ1549 and other HILs frequently show blueshifts that can reach several thousand km s^{-1} (Gaskell 1982; Tytler and Fan 1992; Brotherton et al. 1994; Marziani et al. 1996) indicating the presence of winds or outflows. Dynamics conditions change along the 4DE1 sequence (Bachev et al. 2004) with the HIL blueshift becoming weaker as one proceeds to less FeII strong quasars with broader lines.

3.2 Physical conditions of the BLR

Line widths increase with increasing ionization potential and higher ionization lines usually respond more rapidly to continuum changes. This indicates an "ionization stratification" within the BLR (Peterson

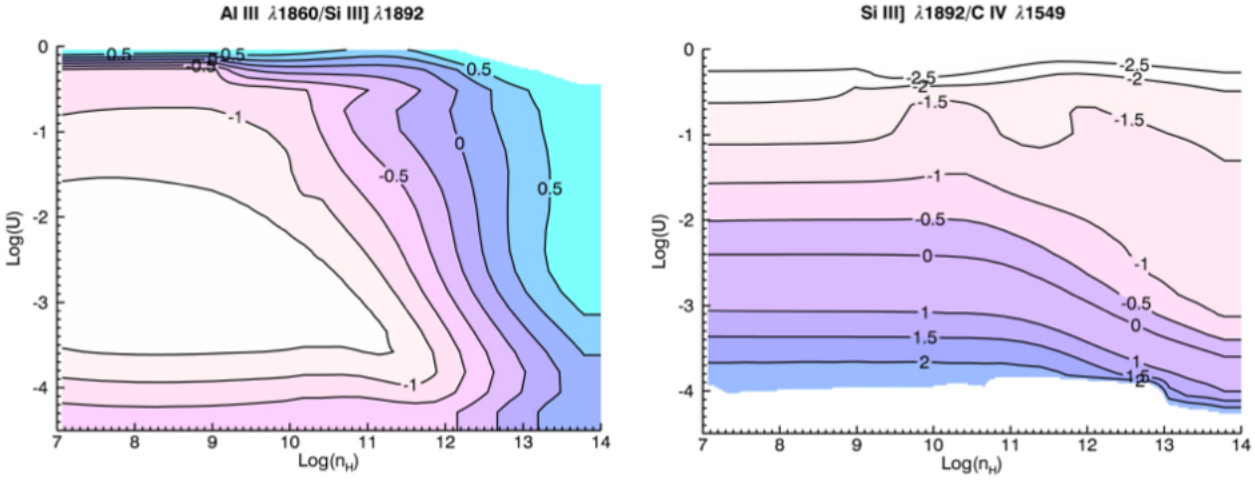

Fig. 1 Behavior of log Si III]λ1892/C IVλ1549 and log Al IIIλ1860/Si III]λ1892 in the 2D parameter space defined by ionization parameter U and hydrogen density $n_{\rm H}$, from a set of 551 simulations that assume solar metallicity, a standard AGN continuum, and $N_{\rm c} = 10^{23}$ cm^{-2}. Two arrays of the Negrete et al. (2012) simulations are shown here to illustrate two cases in which a single line ratio defines a clear trend: Al IIIλ1860/Si III]λ1892 for density, Si III]λ1892/C IVλ1549 for ionization parameter (if density is less than the critical density of Si III]λ1892).

and Wandel 1999). The stratification is also empirically confirmed by the simultaneous presence of strong C III]λ1909 and Si III]λ1892 representing transitions involving critical densities differing by more than one order of magnitude. This makes the search for a single solution in terms of density and ionization rather ambiguous. Nonetheless, Eq. 1 can be used to estimate the ionizing photon flux, i.e., the product $n_{\rm H}U$, as we will discuss below.

Negrete et al. (2013) studied a sample of 13 type-1 AGNs with high-quality HST/FOS coverage in the range 1200 – 2000 Å, and with $c\tau$ measures for Hβ from monitoring campaigns (Bentz et al. 2013). These authors obtained two different solutions for $n_{\rm H}U$ depending on whether C III]λ1909 or Al IIIλ1860 was used: in the first case the solution involved high ionization and low density and in the second high density and low ionization. These solutions were compared with the ones derived using reverberation mapping i.e., setting $c\tau \approx r_{\rm BLR}$ in Eq. 1, where the time lag $\tau_{\rm L}$ represents the light travel time for continuum photons to reach the broad line region. Only the high-density solution showed good agreement with $c\tau_{\rm L}$. C III]λ1909 yields systematically lower $n_{\rm H}U$ which is a result that can be easily understood in terms of stratification within the BLR or other more complex scenarios (Maiolino et al. 2010).

3.3 Physical conditions at the 4DE1 extremes

At the extremes of the 4DE1 sequence physical conditions appear better defined and it is possible to derive a typical density and ionization parameter for the BLR. At the high $R_{\rm FeII}$ end of the 4DE1 sequence (extreme Population A) we find sources whose optical spectra are dominated by LIL emission. In the UV such sources show large HIL blueshifts and weak C III]λ1909. They are interpreted as sources radiating close to the Eddington limit with HILs mostly reflecting high-ionization winds. Using the diagnostic line ratios described in §2, Negrete et al. (2012) find well defined physical conditions: low ionization ($U \lesssim 10^{-2}$) and high density ($10^{12} - 10^{13}$ cm^{-3}) with an uncertainty less than $\pm$ 0.3 dex along with significant metal enrichment. The weakness of C III]λ1909 enables all important emission line ratios to converge toward a high-density solution. Extreme $R_{\rm FeII}$ sources show low equivalent width in *all* the strongest broad emission lines i.e, C IVλ1549 and Balmer lines: extreme Eddington ratio sources may have stripped the BLR of lower column density gas, leaving only the densest part of the BLR (Negrete et al. 2013). These sources show extreme iron and aluminium emission which might be associated with chemical enrichment (Juarez et al. 2009); selective aluminium and silicon abundance enhancement may be needed to explain in detail the observed emission line ratios (Negrete et al. 2012).

At the Population B end of the 4DE1 sequence most sources show weak optical Fe II emission as well as very weak or undetectable Al IIIλ1860 i.e., Al IIIλ1860 / C III]λ1909 $\rightarrow$ 0. Many of these sources are radio loud. 3C 390.3 shows complex line profiles including a prominent blue hump in the Balmer lines and HILs.

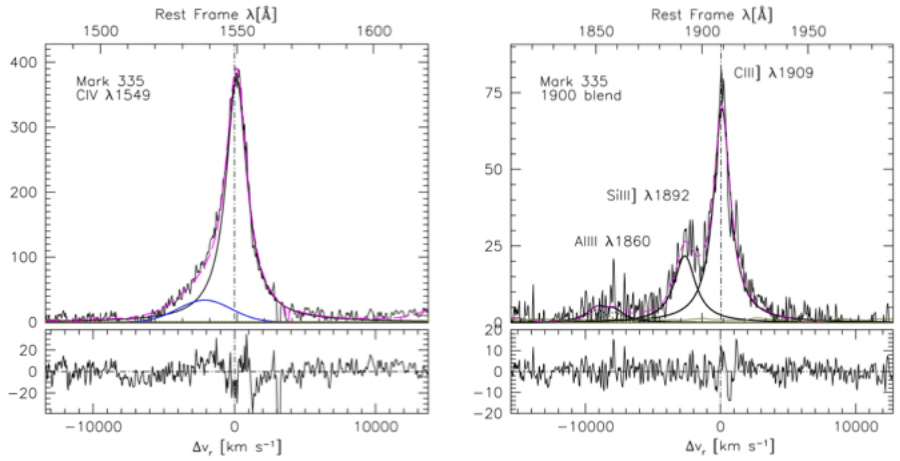

Fig. 2 Analysis of relevant blends for Mark 335. Left panel: the CIVλ1549 line profile is fit using a scaled Hβ profile (black line), symmetric and almost unshifted whose width can serve as estimator of virial broadening; the residual on the blue side is the excess component attributed to a wind or outflow. Right panel: the thick lines represent the features in the blend: doublet AlIIIλ1860, and single lines SiIII]λ1892, CIII]λ1909. UV FeII and FeIII (grey line close to 0) emissions are barely detectable in this object.

The blue hump (which is unlikely to be the broad component because of the large shift) shows AlIIIλ1860/ CIII]λ1909 $\approx$ 0.05 while only an upper limit can be assigned to optical Fe II emission. In this case there is no high-density solution. The measured emission line ratios converge toward a low-density solution that also accounts for the observed AlIIIλ1860 / CIII]λ1909 ratio: $\log(n_{\rm H}U) \approx 8.55 \pm 0.14$ at 1σ. We can estimate $n_{\rm H}$ and U separately (not just their product): $\log(n_{\rm H}) \approx 9.95 \pm 0.13$ and $\log(U) \approx -1.40 \pm 0.12$ at 1σ (Negrete et al. 2014).

3.4 Chemical abundances of the BLR gas

The diagnostic ratio (SiIVλ1397+ OIV]λ1402) / CIVλ1549 can be most easily used for metallicity estimation. Other ratios like NVλ1240/ HeIIλ4686 may be stronger indicators (Ferland et al. 1996) but are more difficult to measure since e.g. NVλ1240 is heavily blended with Lyα. The 4DE1 sequence is likely a sequence of ionization in the sense of a steady decrease in prominence of the low-ionization emission towards Population B. Metallicity might also play a role: Z may be highly super-solar especially for extreme Pop. A sources i.e. when FeII is stronger than Hβ then decreasing to solar or slightly super-solar values in Pop. B sources (Shin et al. 2013; Sulentic et al. 2014.

4 Radius of BLR and black hole mass

If we know *the product of* $n_{\rm H}$ and U then we can estimate $r_{\rm BLR}$ by inverting Eq. 1:

$$r_{\rm BLR} = \text{const.}(Un_{\rm H})^{-\frac{1}{2}} \left(\int_{\nu_0}^{+\infty} \frac{L_\nu}{h\nu} d\nu \right)^{\frac{1}{2}} \quad (2)$$

where the first and second bracketed factors represent the physical conditions and the number of ionizing photons respectively. This technique has been applied by several authors in past decades (Padovani et al. 1990; Wandel et al. 1999). The recent analysis of Negrete et al. (2013) showed that there is very good agreement between $r_{\rm BLR}$ estimates based on the photon flux and $c\tau$ – most likely better than estimates obtained from the correlation between $c\tau$ and luminosity ($c\tau \propto L_\lambda^a$ where $a = 0.5 - 0.7$, with $a \approx 0.53$; Bentz et al. 2013), on which virial black hole mass estimates in high redshift quasars are based(e.g., Shen and Liu 2012).

4.1 Implications for the virial broadening estimator

The Hβ profile is unshifted within $\pm$ 200 km s^{-1} and symmetric in most Pop. A sources. Measurements of the Hβ (or MgIIλ2800) line width are therefore considered the safest virial broadening estimator and was recently confirmed for $\approx$ 80 % of Pop. A sources. Population B sources show more complex profiles where often shows Hβ redshifts and redward asymmetries (Punsly 2010; Marziani et al. 2013). Shift amplitudes are however modest with shift/width ratios typically below 0.2 allowing one to extract a reasonable virial broadening estimator also for Pop. B sources. In order to account for non-virial motions in the integrated line profiles it has proven effective to isolate three line profile components: (1) an almost unshifted and symmetric broad

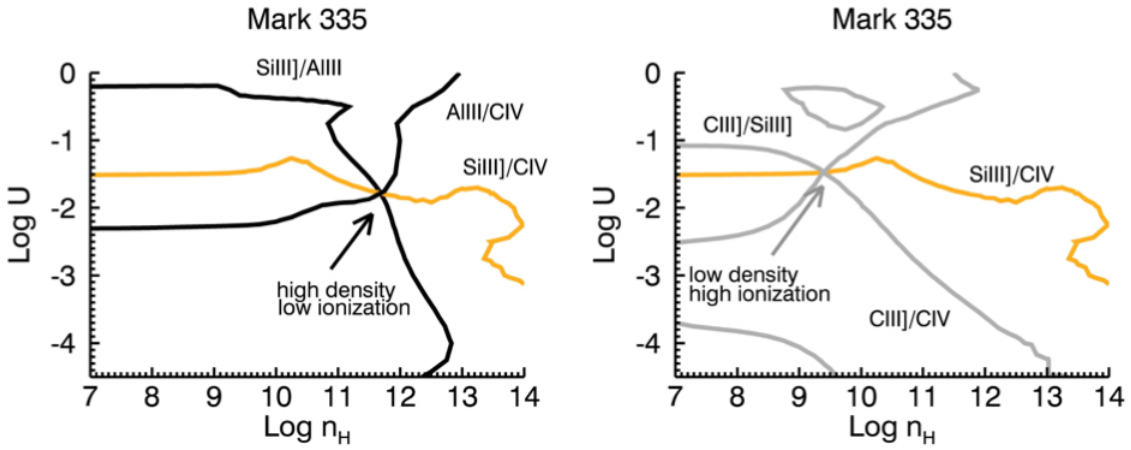

Fig. 3 The parameter plane $U - n_{\rm H}$, with isopleths of constant emission line ratio, for the case of Mark 335. Left panel: high density, low ionization solution; right: low density, high ionization solution. Black and grey lines trace ratios involving CIII]λ1909 and AlIIIλ1860 respectively. See text for more details.

component (BC) assumed to be broadened by virial motion, (2) an occasional blueshifted component (similar to CIV) due to gas outflows and (3) for Pop. B only, a very broad component (VBC) involving the Hβ emitting region that produces no FeII. The VBC can be interpreted as arising in the innermost (highest ionization) part of the Balmer line emitting region (Hu et al. 2012).

A measure of the BC component width in UV lines other than CIVλ1549 and Lyα is needed to facilitate black hole mass measurements for high redshift quasars. The CIVλ1549 profile width is unreliable for $M_{\rm BH}$ estimates, especially for Pop. A sources (Netzer et al. 2007; Sulentic et al. 2007; Fine et al. 2010), and Lyα is frequently contaminated by absorption features. Negrete et al. (2013) and Negrete et al. (2014) recently compared HST archival spectra and optical observations for several type-1 AGNs. These authors verified that BC FWHM measures for Hβ are in very good agreement with FWHM measures for SiIII]λ1892 and AlIIIλ1860 that can be considered as the best virial broadening estimators in the far UV along with MgIIλ2800 (Trakhtenbrot and Netzer 2012; Marziani et al. 2013, and references therein). The virial $M_{\rm BH}$ mass can then be computed taking into account that the structure factor is also changing along eigenvector 1 (Collin et al. 2006).

4.2 The case of Mark 335

Mark 335 (PG 0003+199) is a low-z quasar with archival FOS observations as well as extensive monitoring that has lead to an accurate cross correlation lag estimate, $\log c\tau \approx 16.61$ [cm] (Kaspi et al. 2000; Kollatschny et al. 2006; Bentz et al. 2013). The CIVλ1549 and CIII]λ1909 spectral ranges are shown in Fig. 2. Analysis of emission line blends is especially straightforward in this case because lines appear to be dominated by the virial BC with only minor CIVλ1549 blueshifted emission. Fig. 2 shows line profiles fit with a Lorentzian function that is appropriate for Population A sources (e.g., Zamfir et al. 2010). Fig. 3 shows the isopleths of constant diagnostic ratios. Their crossing points identify low density ($\log n_{\rm H}U \approx 7.91$ [cm^{-3}], left) and high density solutions ($\log n_{\rm H}U \approx 9.94$ [cm^{-3}], right). The high density solution is close to the one obtained by using the measured $c\tau$ in Eq. 2, $\log n_{\rm H}U \approx 10.39$ [cm^{-3}]. Using Eq. 2 to estimate $\log r$ we obtain 16.83 [cm^{-3}] with a difference of 0.22 dex from the reverberation value (Negrete et al. 2014).

5 MAST Inspection

Unbiased quasar evolution studies on black hole mass, Eddington ratio, and chemical abundances require samples at low and high-z that match their luminosity distributions and that cover the same rest frame range (Willott et al. 2010; Sulentic et al. 2014). The Mikulski Archive for Space Telescope (MAST) provides the backbone for statistical analysis of low-z AGN UV properties and for comparisons with high-z sources. The Palomar Green (Green et al. 1986) survey has played an important role in the analysis of optical observations for low-z, bright quasars. A search of MAST indicates that only 50% of PG sources have usable HST spectra (Shin et al. 2013) while 1/6 have no data at all (Fig. 4). The S/N distribution also indicates that most sources have data whose quality is inferior to available

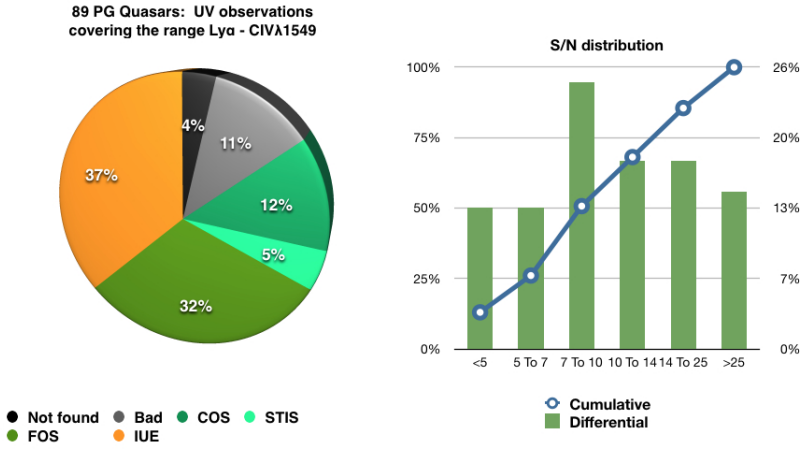

Fig. 4 Left: archival spectroscopic UV observations available for analysis, by instruments, for a sample of 89 PG quasars (data from Shin et al. 2013). Right: differential and cumulative S/N distribution for the available observations.

optical observations. Therefore, the number of low-z sources with high S/N UV spectra is insufficient to yield a pool wide enough to sample the low-z phenomenology with high statistical significance. There is a problem of completeness that is even worse if obscured/type-2 AGNs are considered (e.g., Roig et al. 2014). The relative scarcity of data has a strong impact on our understanding of key issues. Several studies still do not reach a consensus on whether metallicity Z is correlated with luminosity, Eddington ratio, or black hole mass (e.g. Matsuoka et al. 2011; Shin et al. 2013, and references therein). In addition, very few sources have been monitored in the UV where HIL profile changes may be associated to the high-ionization outflow properties.

6 Conclusion

Rest frame UV emission line measures are crucial to our understanding of physical conditions in quasars. They make possible estimates of emitting region radius, black hole mass, Eddington ratio, etc. The 4D Eigenvector 1 formalism allows us to contextualize the diagnostic analysis of sources that are physically and structurally different. Archives from past /present space missions have been extremely valuable in obtaining key information about the inner structure of quasars, most notably strong evidence for significant outflows in a large fraction of sources. Much is still needed in terms of population coverage and data quality in order to address key issues related to metallicity and to outflows that ultimately may provide feedback effects relevant to the evolution of the host galaxies.

References

Bachev, R., Marziani, P., Sulentic, J.W., Zamanov, R., Calvani, M., Dultzin-Hacyan, D.: Astroph. J. **617**, 171 (2004). arXiv:astro-ph/0408334. doi:10.1086/425210

Baldwin, J.A., Ferland, G.J., Korista, K.T., Carswell, R.F., betal: Astroph. J. **461**, 664 (1996). doi:10.1086/177093

Bentz, M.C., Denney, K.D., Grier, C.J., Barth, A.J., Peterson, B.M., et al., : Astroph. J. **767**, 149 (2013). 1303.1742. doi:10.1088/0004-637X/767/2/149

Boroson, T.A.: Astroph. J. **565**, 78 (2002). arXiv:astro-ph/0109317. doi:10.1086/324486

Boroson, T.A., Green, R.F.: Astroph. J. Suppl. **80**, 109 (1992). doi:10.1086/191661

Brotherton, M.S., Wills, B.J., Steidel, C.C., Sargent, W.L.W.: Astroph. J. **423**, 131 (1994). doi:10.1086/173-7194

Brühweiler, F., Verner, E.: Astroph. J. **675**, 83 (2008). doi:10.1086/525557

Collin, S., Kawaguchi, T., Peterson, B.M., Vestergaard, M.: A&Ap **456**, 75 (2006). arXiv:astro-ph/0603460. doi:10.1051/0004-6361:20064878

Davidson, K., Netzer, H.: Reviews of Modern Physics **51**, 715 (1979). doi:10.1103/RevModPhys.51.715

D'Onofrio, M., Marziani, P., Sulentic, J.W. (eds.): Fifty Years of Quasars From Early Observations and Ideas to Future Research. Astrophysics and Space Science Library, vol. 386. Springer, Berlin-Heidelberg (2012). doi:10.1007/978-3-642-27564-7

Ferland, G.J., Baldwin, J.A., Korista, K.T., Hamann, F., *et al.*: Astroph. J. **461**, 683 (1996). doi:10.1086/177094

Ferland, G.J., Hu, C., Wang, J., Baldwin, J.A., *et al.*: Astroph. J. l **707**, 82 (2009). 0911.1173. doi:10.1088/0004-637X/707/1/L82

Ferland, G.J., Porter, R.L., van Hoof, P.A.M., Williams, R.J.R., *et al.*: RevMexA&Ap **49**, 137 (2013). 1302.4485

Fine, S., Croom, S.M., Bland-Hawthorn, J., Pimbblet, K.A., *et al.*: Mon. Not. R. Astron. Soc. **409**, 591 (2010). 1005.5287. doi:10.1111/j.1365-2966.2010.17107.x

Gaskell, C.M.: Astroph. J. **263**, 79 (1982). doi:10.1086-/160481

Gaskell, C.M.: ArXiv e-prints **arXiv0903.4447G** (2009). 0903.4447

Green, R.F., Schmidt, M., Liebert, J.: Astroph. J. s **61**, 305 (1986). doi:10.1086/191115

Grier, C.J., Peterson, B.M., Horne, K., Bentz, M.C., Pogge, R.W., Denney, K.D., *et al.*: Astroph. J. **764**, 47 (2013). 1210.2397. doi:10.1088/0004-637X/764/1/47

Hu, C., Wang, J.-M., Ho, L.C., Ferland, G.J., Baldwin, J.A., Wang, Y.: Astroph. J. **760**, 126 (2012). 1210.4187. doi:10.1088/0004-637X/760/2/126

Juarez, Y., Maiolino, R., Mujica, R., Pedani, M., Marinoni, S., Nagao, T., Marconi, A., Oliva, E.: A&Ap **494**, 25 (2009). 0901.0974. doi:10.1051/0004-6361:200811415

Kaspi, S., Smith, P.S., Netzer, H., Maoz, D., Jannuzi, B.T., Giveon, U.: Astroph. J. **533**, 631 (2000). arXiv:astro-ph/9911476. doi:10.1086/308704

Kollatschny, W., Zetzl, M., Dietrich, M.: Astron. Astrophys. **454**, 459 (2006). doi:10.1051/0004-6361:20054357

Kruczek, N.E., Richards, G.T., Gallagher, S.C., Deo, R.P., *et al.*: Astron. J. **142**, 130 (2011). 1109.1515. doi:10.1088/0004-6256/142/4/130

Kuraszkiewicz, J., Wilkes, B.J., Schmidt, G., Smith, P.S., Cutri, R., Czerny, B.: Astroph. J. **692**, 1180 (2009). doi:10.1088/0004-637X/692/2/1180

Maiolino, R., Risaliti, G., Salvati, M., Pietrini, P., *et al.*: Astron. Astrophys. **517**, 47 (2010). 1005.3365. doi:10.1051/0004-6361/200913985

Marziani, P., Sulentic, J.W., Dultzin-Hacyan, D., Calvani, M., Moles, M.: Astroph. J. Suppl. **104**, 37 (1996). doi:10.1086/192291

Marziani, P., Sulentic, J.W., Zwitter, T., Dultzin-Hacyan, D., Calvani, M.: Astroph. J. **558**, 553 (2001). arXiv:astro-ph/0105343. doi:10.1086/322286

Marziani, P., Sulentic, J.W., Plauchu-Frayn, I., del Olmo, A.: Astron. Astrophys. **555**, 89 (2013). 1305.1096. doi:10.1051/0004-6361/201321374

Matsuoka, K., Nagao, T., Marconi, A., Maiolino, R., Taniguchi, Y.: Astron. Astrophys. **527**, 100 (2011). 1011.5811. doi:10.1051/0004-6361/201015584

Nagao, T., Maiolino, R., Marconi, A.: Astron. Astrophys. **447**, 863 (2006). arXiv:astro-ph/0508652. doi:10.1051/00-04-6361:20054127

Negrete, A., Dultzin, D., Marziani, P., Sulentic, J.: Astroph. J. **757**, 62 (2012). 1107.3188

Negrete, C.A., Dultzin, D., Marziani, P., Sulentic, J.W.: Astroph. J. **771**, 31 (2013). 1305.4574. doi:10.1088/0004-637X/771/1/31

Negrete, C.A., Dultzin, D., Marziani, P., Sulentic, J.W.: Advances in Space Research **54**, 1355 (2014). doi:10.-1016/j.asr.2013.11.037

Netzer, H.: The Physics and Evolution of Active Galactic Nuclei. Cambridge University Press, Cambridge (2013)

Netzer, H., Lira, P., Trakhtenbrot, B., Shemmer, O., Cury, I.: Astroph. J. **671**, 1256 (2007). 0708.3787. doi:10.1086/523035

Padovani, P., Burg, R., Edelson, R.A.: Astroph. J. **353**, 438 (1990). doi:10.1086/168631

Peterson, B.M., Wandel, A.: Astroph. J. l **521**, 95 (1999). arXiv:astro-ph/9905382. doi:10.1086/312190

Peterson, B.M., Ferrarese, L., Gilbert, K.M., Kaspi, S., *et al.*: Astroph. J. **613**, 682 (2004). arXiv:astro-ph/0407299. doi:10.1086/423269

Popović, L.Č., Kovačević, J.: Astroph. J. **738**, 68 (2011). 1106.3021. doi:10.1088/0004-637X/738/1/68

Punsly, B.: Astroph. J. **713**, 232 (2010). 1002.4681. doi:10.1088/0004-637X/713/1/232

Richards, G.T., Kruczek, N.E., Gallagher, S.C., Hall, P.B., *et al.*: Astron. J. **141**, 167 (2011). 1011.2282. doi:10.1088/0004-6256/141/5/167

Roig, B., Blanton, M.R., Ross, N.P.: Astroph. J. **781**, 72 (2014). doi:10.1088/0004-637X/781/2/72

Sameshima, H., Kawara, K., Matsuoka, Y., Oyabu, S., Asami, N., Ienaka, N.: Mon. Not. R. Astron. Soc. **410**, 1018 (2011). 1008.2405. doi:10.1111 / j.1365-2966.-2010.17498.x

Shen, Y., Liu, X.: Astroph. J. **753**, 125 (2012). 1203.0601. doi:10.1088/0004-637X/753/2/125

Shin, J., Woo, J.-H., Nagao, T., Kim, S.C.: Astroph. J. **763**, 58 (2013). 1211.6749. doi:10.1088/0004-637X/-763/1/58

Sigut, T.A.A., Pradhan, A.K.: Astroph. J. Suppl. **145**, 15 (2003). arXiv:astro-ph/0206096. doi:10.1086/345498

Steinhardt, C.L., Silverman, J.D.: Publ. Astron. Soc. Jpn. **65**, 82 (2013). doi:10.1093/pasj/65.4.82

Sulentic, J.W., Marziani, P., Zwitter, T., Dultzin-Hacyan, D., Calvani, M.: Astroph. J. L **545**, 15 (2000). arXiv:astro-ph/0009326. doi:10.1086/317330

Sulentic, J.W., Marziani, P., Zamanov, R., Bachev, R., Calvani, M., Dultzin-Hacyan, D.: Astroph. J. L **566**, 71 (2002). arXiv:astro-ph/0201362. doi:10.1086/339594

Sulentic, J.W., Bachev, R., Marziani, P., Negrete, C.A., Dultzin, D.: Astroph. J. **666**, 757 (2007). 0705.1895. doi:10.1086/519916

Sulentic, J.W., Marziani, P., del Olmo, A., Dultzin, D., *et al.*: ArXiv e-prints (2014). 1406.5920

Tang, B., Shang, Z., Gu, Q., Brotherton, M.S., Runnoe, J.C.: Astroph. J. Suppl. **201**, 38 (2012). 1207.2539. doi:10.1088/0067-0049/201/2/38

Trakhtenbrot, B., Netzer, H.: Mon. Not. R. Astron. Soc. **427**, 3081 (2012). 1209.1096. doi:10.1111/j.1365-2966.2012.22056.x

Tytler, D., Fan, X.-M.: Astroph. J. Suppl. **79**, 1 (1992). doi:10.1086/191642

Vanden Berk, D.E., Richards, G.T., Bauer, A., Strauss, M.A., *et al.*: AJ **122**, 549 (2001). arXiv:astro-ph/0105231. doi:10.1086/321167

Vestergaard, M., Wilkes, B.J.: Astroph. J. Suppl. **134**, 1 (2001). arXiv:astro-ph/0104320. doi:10.1086/320357

Wandel, A., Peterson, B.M., Malkan, M.A.: Astroph. J. **526**, 579 (1999). arXiv:astro-ph/9905224. doi:10.1086/308017

Willott, C.J., Delorme, P., Reylé, C., Albert, L., et , al.: Astron. J. **139**, 906 (2010). 0912.0281. doi:10.1088/0004-6256/139/3/906

Wills, B.J., Laor, A., Brotherton, M.S., Wills, D., Wilkes, B.J., Ferland, G.J., Shang, Z.: Astroph. J. l **515**, 53 (1999). doi:10.1086/311980

Zamfir, S., Sulentic, J.W., Marziani, P., Dultzin, D.: Mon. Not. R. Astron. Soc. **403**, 1759 (2010). 0912.4306. doi:10.1111/j.1365-2966.2009.16236.x

This manuscript was prepared with the AAS LaTeX macros v5.2.